Research Article | Vol. 25, No. 20 | 2 Oct 2017 | OPTICS EXPRESS 23634
Optics EXPRESS

Photonic integration platform with pump free microfluidics

R. THOMAS,[1,3] A. HARRISON,[1] D. BARROW,[2] AND P. M. SMOWTON[1,4]

[1]*School of Physics and Astronomy, Cardiff University, The Parade, Cardiff, CF24 3AA, UK*
[2]*Cardiff School of Engineering, Cardiff University, The Parade, Cardiff CF24 3AA, UK*
[3]*Thomasr25@cardiff.ac.uk*
[4]*SmowtonPM@cardiff.ac.uk*

Abstract: Chip based particle sensing using 3D capillary fill microfluidics integrated with monolithically integrated lasers and photodetectors is used to demonstrate the feasibility of true chip scale photonic measurements of fluids. The approach is scalable and manufactured using industry standard compound semiconductor fabrication tools. The need for fluid speed regulation via external pumps is removed by measuring local particle velocity at the point of interrogation and particle position within the fluid flow is derived from multiple time resolved forward scattered light signals. Particle size discrimination of 10 and 15 μm polystyrene microbeads is used as an example.

OCIS codes: (250.0250) Optoelectronics; (250.5960) Semiconductor lasers; (250.5300) Photonic integrated circuits; (280.4788) Optical sensing and sensors; (280.2490) Flow diagnostics.

References and links

1. D. Psaltis, S. R. Quake, and C. Yang, "Developing optofluidic technology through the fusion of microfluidics and optics," Nature **442**(7101), 381–386 (2006).
2. C. Monat, P. Domachuk, and B. J. Eggleton, "Integrated optofluidics: A new river of light," Nat. Photonics **1**(2), 106–114 (2007).
3. H. Schmidt and A. R. Hawkins, "The photonic integration of non-solid media using optofluidics," Nat. Photonics **5**(10), 598–604 (2011).
4. X. Fan and I. M. White, "Optofluidic Microsystems for Chemical and Biological Analysis," Nat. Photonics **5**(10), 591–597 (2011).
5. M. Boyd-Moss, S. Baratchi, M. Di Venere, and K. Khoshmanesh, "Self-contained microfluidic systems: a review," Lab Chip **16**(17), 3177–3192 (2016).
6. J. C. T. Eijkel and A. van den Berg, "Young 4ever-the use of capillarity for passive flow handling in lab on a chip devices," Lab Chip **6**(11), 1405–1408 (2006).
7. B. Helbo, A. Kristensen, and A. A. Menon, "A micro-cavity fluidic dye laser," J. Micromech. Microeng. **13**(2), 307–311 (2003).
8. S. Balslev and A. Kristensen, "Microfluidic single-mode laser using high-order Bragg grating and antiguiding segments," Opt. Express **13**(1), 344–351 (2005).
9. M. C. Gather and S. H. Yun, "Single-cell biological lasers," Nat. Photonics **5**(7), 406–410 (2011).
10. M. Schubert, K. Volckaert, M. Karl, A. Morton, P. Liehm, G. B. Miles, S. J. Powis, and M. C. Gather, "Lasing in Live Mitotic and Non-Phagocytic Cells by Efficient Delivery of Microresonators," Sci. Rep. **7**, 40877 (2017).
11. S. W. Kettlitz, S. Valouch, W. Sittel, and U. Lemmer, "Flexible planar microfluidic chip employing a light emitting diode and a PIN-photodiode for portable flow cytometers," Lab Chip **12**(1), 197–203 (2012).
12. X. J. Liang, A. Q. Liu, C. S. Lim, T. C. Ayi, and P. H. Yap, "Determining refractive index of single living cell using an integrated microchip," Sens. Actuat. A **133**(2), 349–354 (2007).
13. R. Nagarajan, M. Kato, J. Pleumeekers, P. Evans, S. Corzine, A. Dentai, S. Murthy, M. Missey, R. Muthiah, R. A. Salvatore, C. Joyner, R. Schneider, M. Ziari, F. Kish, and D. Welch, "InP Photonic Integrated Circuits," IEEE J. Sel. Top. Quantum Electron. **16**(5), 1113–1125 (2010).
14. S. Cran-McGreehin, T. F. Krauss, and K. Dholakia, "Integrated monolithic optical manipulation," Lab Chip **6**(9), 1122–1124 (2006).
15. S. Chen, W. Li, J. Wu, Q. Jiang, M. Tang, S. Shutts, S. N. Elliott, A. Sobiesierski, A. J. Seeds, I. Ross, P. M. Smowton, and H. Liu, "Electrically pumped continuous-wave III–V quantum dot lasers on silicon," Nat. Photonics **10**(5), 307–311 (2016).
16. K. V. Nemani, K. L. Moodie, J. B. Brennick, A. Su, and B. Gimi, "In vitro and in vivo evaluation of SU-8 biocompatibility," Mater. Sci. Eng. C **33**(7), 4453–4459 (2013).

#302118 https://doi.org/10.1364/OE.25.023634
Journal © 2017 Received 14 Jul 2017; revised 16 Aug 2017; accepted 27 Aug 2017; published 18 Sep 2017

Optics EXPRESS

17. M. Hochberg, N. C. Harris, R. Ding, Y. Zhang, A. Novack, Z. Xuan, and T. Baehr-Jones, "Silicon photonics: the next fabless semiconductor industry," IEEE Solid-State Circuits Magazine **5**(1), 48–58 (2013).
18. F. J. Blanco, M. Agirregabiria, J. Garcia, J. Berganzo, M. Tijero, M. T. Arroyo, J. M. Ruano, I. Aramburu, and K. Mayora, "Novel three-dimensional embedded SU-8 microchannels fabricated using a low temperature full wafer adhesive bonding," J. Micromech. Microeng. **14**(7), 1047–1056 (2014).
19. R. Meier, V. Badilita, U. Wallrabe, and J. G. Korvink, "Processing of 3D multilevel SU-8 fluidic network assisted by PerMX dry-photoresist lamination," NEMS **2012**, 5–8 (2012).
20. Y. Chuang, F. Tseng, J. Cheng, and W. Lin, "A novel fabrication method of embedded micro-channels by using SU-8 thick-film photoresists," Sens. Actuators A Phys. **103**(1-2), 64–69 (2003).
21. A. Rammohan, P. K. Dwivedi, R. Martinez-Duarte, H. Katepalli, M. J. Madou, and A. Sharma, "One-step maskless grayscale lithography for the fabrication of 3-dimensional structures in SU-8," Sens. Actuators B Chem. **153**(1), 125–134 (2011).
22. J. M. Dykes, D. K. Poon, J. Wang, D. Sameoto, J. T. K. Tsui, C. Choo, G. H. Chapman, A. M. Parameswaren, and B. L. Gray, "Creation of embedded structures in SU-8," Proc. SPIE **6465**, 1–11 (2007).
23. G. M. Lewis, P. M. Smowton, P. Blood, and W. W. Chow, "Effect of tensile strain/well-width combination on the measured gain-radiative current characteristics of 635 nm laser diodes," Appl. Phys. Lett. **82**(10), 1524–1526 (2003).
24. I. Karomi, P. M. Smowton, S. Shutts, A. B. Krysa, and R. Beanland, "InAsP quantum dot lasers grown by MOVPE," Opt. Express **23**(21), 27282–27291 (2015).
25. A. Sobiesierski, R. Thomas, P. Buckle, D. Barrow, and P. M. Smowton, "A two-stage surface treatment for the long-term stability of hydrophilic SU-8," Surf. Interface Anal. **47**(13), 1174–1179 (2015).
26. L. Wang, L. A. Flanagan, N. L. Jeon, E. Monuki, and A. P. Lee, "Dielectrophoresis switching with vertical sidewall electrodes for microfluidic flow cytometry," Lab Chip **7**(9), 1114–1120 (2007).

1. Introduction

Tremendous progress has been made in the past few years in the class of devices that combines optics and fluidics demonstrating optical devices that are reconfigurable using fluid properties, optical devices to sense fluidic properties and the detection of particles flowing in fluids [1–4]. For portable, low cost diagnostics and monitoring in point of use and resource poor settings the integration of all components on chip is highly advantageous and 'self-contained' microfluidic systems that remove the dependence on ancillary equipment by incorporating all the components necessary for complete analysis onboard the microfluidic chip is a current focus [5].

Microfluidics driven by capillary action provides a passive means of maneuvering fluids on-chip without the need for external pumps. However, implementation is not simple as the fluid flow is less controlled than with an external pump and, as the quantity of fluid being pulled by the surface forces at the fluid front increases, the fluid velocity decreases with time. Stop / start control of fluid flow can be achieved by abruptly changing channel dimension and fluid velocity can be controlled by continuously changing channel dimensions [6] but this can be impractical for large channel lengths. For fluids containing particles, control of the particle position within the fluid flow is also limited due to the lack of external control of the hydrodynamic forces. In what follows we monitor particle velocity using optical devices and correct for particle position.

While much progress has been made, the light source has been particularly challenging to include on-chip as most of the fluidic and optical guiding functionality has been developed in optically passive materials such as polydimethylsiloxane (PDMS), glass or Silicon. Reports of lasers that have been successfully integrated on chip include those utilizing fluid dyes [7,8] and the exciting work using cells containing Green Fluorescent Protein as the gain medium, in "living lasers" for bio-sensing, could also be integrated in a similar manner [9,10]. While demonstrating excellent performance and sensing capabilities these lasers still require an external optical pump.

Here we propose and demonstrate the feasibility of an approach based on combining an active semiconductor substructure, for on-chip electrically driven reconfigurable lasers and detectors, integrated with capillary fill microfluidics, where fluid velocity is monitored at the interrogation point, all created with industry standard fabrication equipment.

Using semiconductor industry standard approaches for fabricating optical sources and detectors from a single epitaxial wafer naturally leads to an integrated chip solution and

Optics EXPRESS

removes the expensive and time consuming step of manual alignment that transferring active devices to a separate platform would introduce. As evidenced by the silicon industry it also provides the opportunity to scale, while maintaining the precise positioning and without increasing the time for manufacturing. The alternative 'pick and place' style fabrication [11,12] is less useful for more complex systems where multiple aligned devices are required. Monolithic integration up to wafer scale can be used to integrate very large numbers of emitters and detectors [13,14] and the alignment and density of optical elements that can be achieved offers added performance and device functionality. Integration of components on-chip reduces the dependence on external equipment leaving only the fluidics (see later) and the electronics required to drive the laser and detectors. We envisage that in the future, the electronics will also be integrated on chip, through recent developments in direct growth of compound semiconductors on silicon [15] or through vicinal photonics / electronics using e.g. through-silicon vias or bump solder bonding [16]. The use of silicon as a base for subsequent growth of compound semiconductors would also facilitate the scale up of wafer diameter to values typically seen in the Silicon industry and the concomitant significant reduction in cost.

In this paper we introduce a methodology for combining capillary fill microfluidics with compound semiconductor photonic integrated circuits to enable self-contained microfluidic systems using techniques that are compatible with wafer scale manufacturing. Specifically, we describe the design and fabrication of a photonic integrated particle detector and, as an example, demonstrate how 10 μm and 15 μm diameter microbeads in a mixed sample, travelling in a capillary flow, can be differentiated. This example illustrates one way the optofluidic platform we describe could be utilised to support much of the more advanced body of work in optofluidic diagnostics e.g [2,4].

2. Materials and methods

The embedded microfluidics are fabricated from Microchem SU-8 photo-epoxy, chosen for its transparency over much of the visible and near infrared wavelength regime, its biocompatibility [17] and its capacity to be patterned into thick, near vertical features over deep etched surfaces. Several methods exist for creating 3D structures in SU-8. These techniques typically fall into one of two main categories: i) additive methods, where the 3D structure is built up layer by layer using an inter-layer bonding technique, e.g. adhesive wafer bonding [18] and lamination [19], or, ii) dose control methods, where a 3D structure can be formed in a single layer by manipulating the penetration depth of the exposing radiation. This can be achieved with: reflecting/anti-reflecting layers incorporated on the substrate [20], greyscale lithography [21], or, with the use of multiple light sources emitting at different wavelengths [22]. For ease of manufacture and scalability we believe dosage control methods offer a more promising route toward integration of microfluidics with photonics. In this work we introduce an alternative dose control method that utilises spectral filters to select the different emission lines of a single mercury arc lamp. The advantage of this approach is that it can be used to produce wafer scale 3D structures in a single layer of SU-8 using a conventional photolithography mask aligner.

By utilising compound semiconductors the optically active region of the chip can consist of many epitaxially grown layers encompassing a wide range of functionality including, for example, light source, modulator, amplifier and detector. To demonstrate the integration concept we use a relatively simple p-i-n diode structure that can be configured as a laser or a detector. It consists of a single GaInP/AlGaInP quantum well grown within an optical waveguide core and clad with p and n-doped AlInP to create optical guiding in the vertical direction. These layers are grown on an n-doped GaAs substrate and capped with a p-doped GaAs contact layer [23]. The example chosen operates around 635nm wavelength but by choosing alternative active materials such as InP or InAsP quantum dots the operating wavelength range can be varied, or can encompass simultaneously, wavelengths between 630 and 780nm [24] and beyond. 10 μm wide ridges are plasma etched into the surface of the

Optics EXPRESS

semiconductor material and p and n-contact metal electrodes are patterned on to the upper surface to facilitate electrical biasing, see Fig. 1. Under positive electrical bias the ridge encompassing the p-i-n diode operates as a laser and under zero or negative electrical bias it operates as a detector.

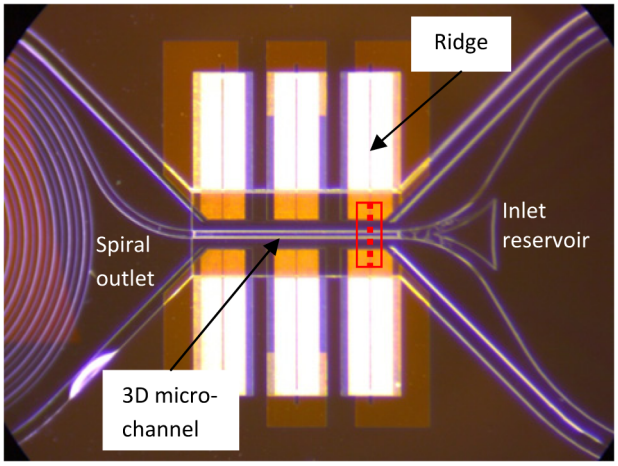

Fig. 1. Plan view of an integrated chip with a ridge laser/detector and the key components of the SU-8 capillary fill microfluidics indicated. The red box indicates the region of interest shown in cross section in Figs. 2 and 3.

In its simplest form the capillary fill fluid delivery system is made up of three main parts: 1) an Inlet reservoir, into which sample fluids are deposited, 2) an embedded 3D micro-channel that promotes laminar flow through the interrogation region, and 3) an outlet reservoir consisting of an open topped spiral channel that provides a sustained pull through of fluid for upwards of 100 s. The spiral acts as a repository for the fluid and the particles it contains, which can be utilised for subsequent analysis. Alternatively, at the time of fabrication, the output channel can be connected externally for longer duration fluid flow. The first option is used here.

To accommodate the on-chip microfluidics, a 15 μm deep foundation channel is etched through the compound semiconductor vertical optical waveguide and into the semiconductor substrate between the paired lasers and detectors using a 5% dilution of H_2O_2/NH_3. This is done so that the centre-line of the channel will intersect the optical axes of the lasers and detectors see Fig. 2.

Optics EXPRESS

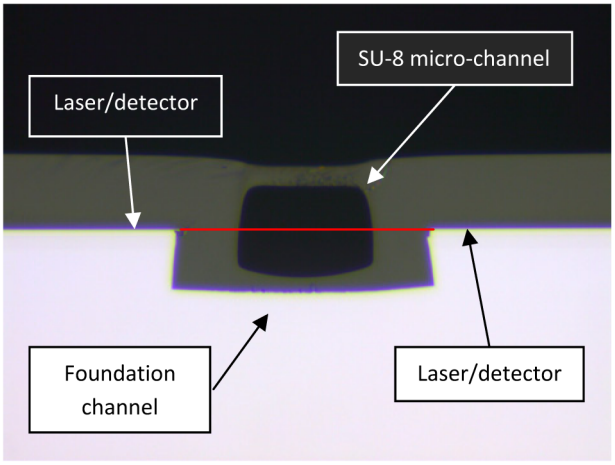

Fig. 2. Cross-section view at the position indicated in Fig. 1 of the interrogation region of the chip. The red line indicates the position of the common optical axis of the laser and photo-detector relative to the fluid channel.

The SU-8 microfluidics are applied to the substrate by spin coating, and patterned with UV exposure from a Karl Zuss MJB3 mask aligner. A 5 μm thick base layer of SU-8 3005 is patterned over the foundation channel to act as an adhesion layer for the subsequent microfluidics and to provide electrical isolation and physical separation from the GaAs substrate. The 3D microfluidics are applied in a single 30 μm thick layer of SU-8 2050. The walls of the structure are patterned using a Hoya 370 nm long pass filter; at longer wavelengths SU-8 is only partially absorbing and so the light penetrates all the way to the bottom of the layer creating a near vertical exposure profile. The roof of the channel is patterned with an Asahi-spectra 340 nm band pass filter which isolates the 334 nm emission line of the mercury lamp; at this wavelength SU-8 is highly absorbing so the light penetrates only a short distance into the layer. Cross-linking of the exposed epoxy is completed with a post exposure bake and immersion in Microposit EC solvent. Unexposed SU-8 is developed away leaving the inlet and outlet reservoirs connected via the embedded 3D micro-channel. The channel has cross sectional dimensions of 25 μm in height by 50 μm in width and a roof thickness of approximately 8 μm.

In its native state SU-8 is insufficiently hydrophilic to enable capillary flow through the embedded channel. It is therefore necessary to modify the surface of the SU-8. We choose to use a two stage treatment consisting of exposure of the surface to an oxygen plasma which renders it hydrophilic, followed by immersion in ethanolamine which extends the duration of the effect to in excess of 3 months [25]. The application of the surface treatment enables capillary flow through the embedded channel for water or alcohol based fluids

3. Operation

The laser sections of the chip are operated in pulsed mode at a repetition rate of 10 kHz with a pulse length of 500 ns. At this duty cycle any current induced self-heating is not observable, even though the laser output intensity is very sensitive to temperature changes, and the operating temperature of the chip is taken to be constant. Each section is electrically forward biased in sequence, so that while one section acts as a laser the others can be operated as photo-detectors. The resulting photo-voltages are recorded through a data logger. A particle passing through a laser beam causes a perturbation to the forward scattered light as seen on the detector across the channel, see Fig. 3. The fluid speed provided by the capillary action is such that for a 10um diameter particle the transit time of the particle is typically around 50

Optics EXPRESS

times slower than the period between pulses so the transit event is captured as a series of discrete photo-voltage measurements on each of the paired laser/detectors.

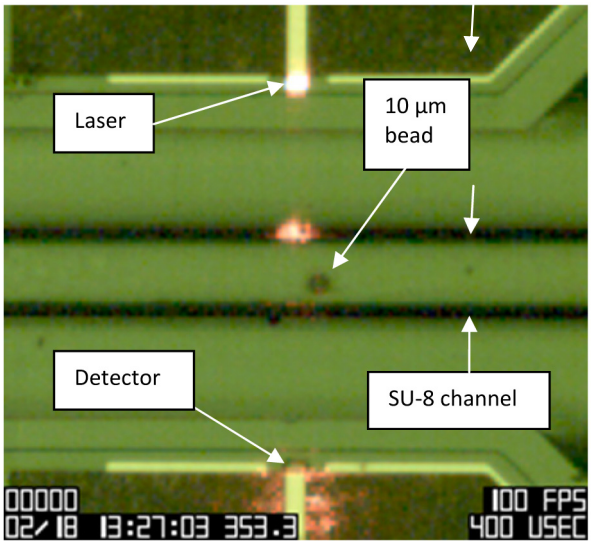

Fig. 3. High speed camera image of a micro-bead passing through the fluid channel between the first integrated laser-detector pair as indicated in Fig. 1. Note the scattered red laser light from the side walls of the micro-channel and at the front edge of the detector, which simply reduces the intensity available for measurement.

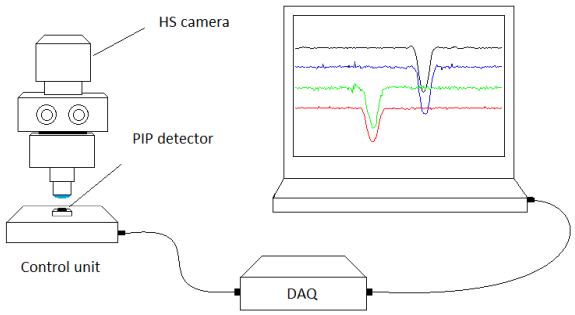

Fig. 4. A schematic diagram of the experimental set up used to measure bead detection events. The time resolved transit of a particle is recorded on two adjacent laser/detector pairs producing four inter-leaved time traces (coloured lines).

By operating the lasers in sequence they are effectively toggled back and forth on alternate pulses and the laser beam transit events are captured from both sides of the channel in separate but interleaved time traces. Traces from opposing sides of the channel are then averaged in order to compensate for lateral variations in particle position. The traces from adjacent laser/detector pairs are measured sequentially so that a particle's time of flight between known fixed points along the length of the channel can be measured.

The chip is plugged directly into a control unit that contains the electronics required to sequence and drive the lasers and sample and amplify the photo-voltage signals. The control unit is designed with a low profile so that it can be operated within the working distance of a microscope objective lens. This allows the passage of particles to be recorded independently of the chip based measurement using a high speed camera (Mega Speed Corp.), see Fig. 4. The camera and microscope are used here to characterise the performance of the chip and are

Optics EXPRESS

not a requirement of the final system. The amplified detector outputs are logged externally with a NI 6210 USB data acquisition board (DAQ) and the data from both the DAQ and high speed camera are recorded to a laptop computer. For a completely self-contained system we envisage that the functionality of the DAQ and control electronics can be integrated on-chip and the laptop can be replaced by a smart phone.

By measuring time resolved particle transits at two different points along the length of the channel, the local velocity can be determined with an accuracy determined by the timing precision of the electronics and the positional accuracy of optical lithography. This allows the use of capillary fill microfluidics for particle delivery to sensing elements, where particle velocity at the point of interrogation is not controlled externally but is measured.

4. Results and discussion

As a simple demonstration we use a (2.0 ± 0.2) μL volume of mixed 10 and 15 micron (± 10%) calibration beads, which was deposited in the inlet reservoir and 100 s of data was recorded from two adjacent laser/detector pairs spaced 30 μm apart along the length of the micro-channel. The resulting photo-voltage signals are plotted in Fig. 5 (only 30s of data has been included here so that the magnitude and frequency of events are clear).

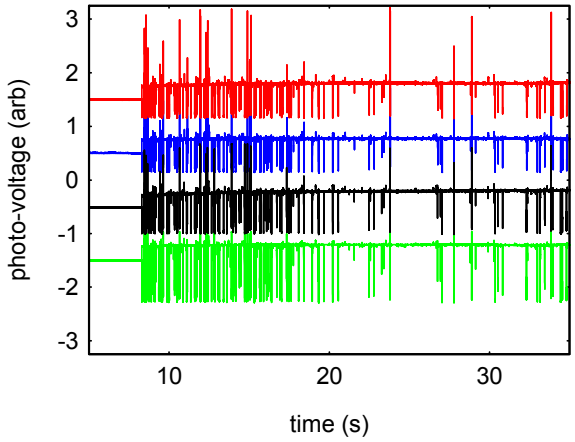

Fig. 5. Normalised photo-voltage signals from two adjacent laser/detector pairs for a mixed sample of 10 and 15 μm beads. The spikes in the data correlate to individual bead transit events.

The step change in the background voltage of the four channels which occurs at around 8 s, is a result of the initially empty channel filling with water. The presence of water in the channel increases the refractive index of the gap between the laser and detector pairs which reduces the reflectivity of two interfaces, according to Fresnel's law of reflection, improving the coupling between them thus increasing the background voltage detected. As this event is common to all laser/detector pairs, the voltage step can and has been used to normalize the signal levels. Bead transit events appear in Fig. 5 as a series of sharp spikes and each event is captured on all four channels. In Fig. 6 the time resolved signals of the four detector channels are plotted for the transit of a single bead. The signals in black and green consist of multiple points spaced by 100 μs as the devices are switched from laser / detector to detector / laser and then on to the next pair of devices. As the bead passes through the interrogation region from one side to the other, it perturbs the adjacent laser/detectors pairs one after the other.

Optics EXPRESS

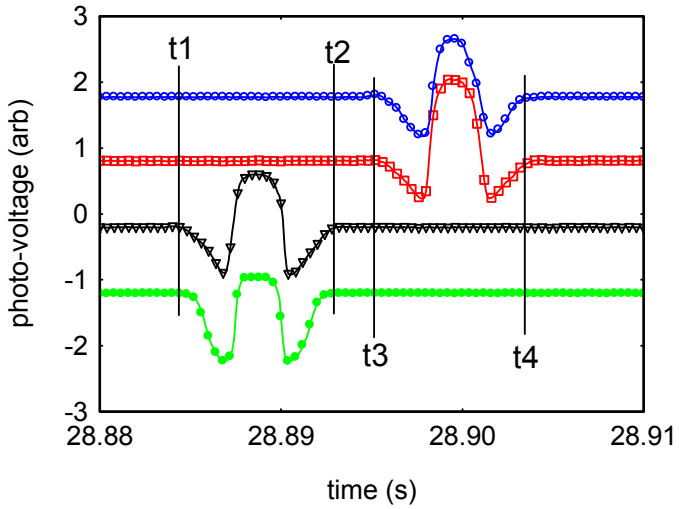

Fig. 6. A single bead transit as captured in the four detector photo-voltage signals with vertical black lines indicating the times that are taken to be the start and end of the laser beam-microbead interaction. Note, every tenth data point is shown on the detector traces.

The time taken for the leading (trailing) edge of the particle to pass the front (back) edges of the adjacent laser beams are $\Delta tp = (t3 - t1)$ and $(t4 - t2)$. These intervals are determined by the pitch of the laser beams, $p = (30.0 \pm 0.5)$ μm only and not their widths or the size of the particle. Dividing the laser beam pitch by either of these time intervals therefore provides a measure of the particle's velocity, v. The measured velocities of 101 transit events over a 30 second period are plotted in Fig. 7. There is no significant difference for the beads of different sizes (method to differentiate these follows). The velocity decreases with time, which emphasises the need for local velocity measurement when utilising capillary flow.

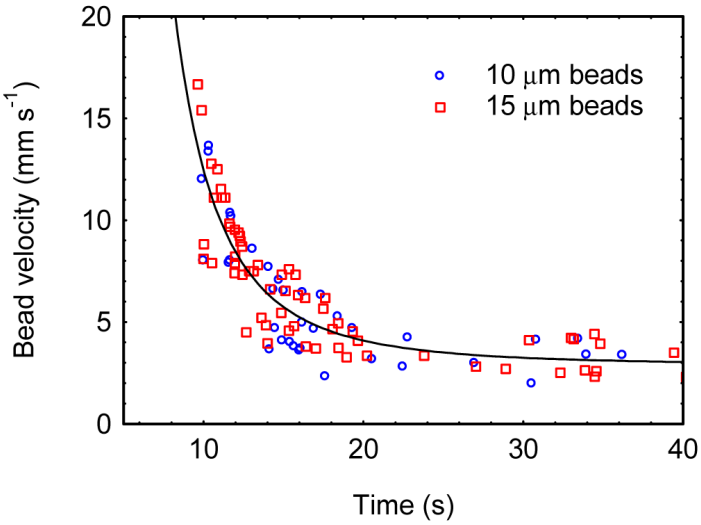

Fig. 7. Bead velocity measured as a function of experiment duration for 10 and 15 um diameter beads.

The time taken for the particle to fully traverse either of the beam pairs i.e. from $\Delta t_w = (t1$ to $t2)$ or $(t3$ to $t4)$, results from a convolution of the particle with the beam. The sum of the

Optics EXPRESS

particle diameter, d, and the beam width, w, therefore equals to the product of this time span and the particle's velocity:

$$d = v.\Delta t_w - w = \left(p \times \frac{\Delta t_w}{\Delta t_p} \right) - w \quad (1)$$

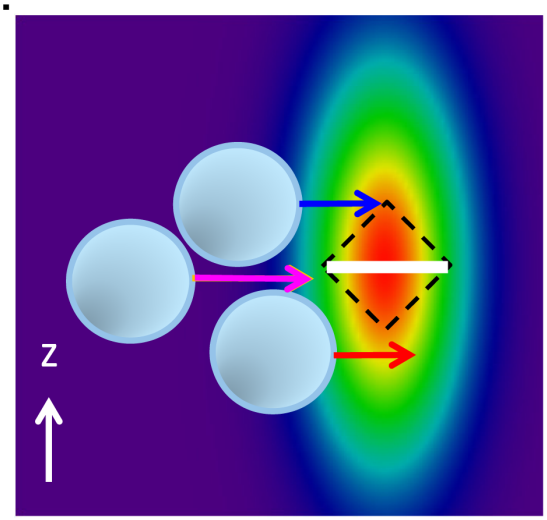

Fig. 8. A colour map of the elliptical farfield distribution of the lasers with a single line of white pixels indicating the central optical axis and representing the area subtended by the detector. The dashed black lines indicate the extent of the system response function that is used to determine the best fit to the bead size histogram data later on.

Before considering the results we should note that the width of the beam is complicated by the elliptical far-field distribution of the lasers and the fact that particles can travel at varying heights. This means that the beam width presented to a particle at the point of measurement is a function of the particle height in the channel. This is represented schematically in Fig. 8. In fact for particle sizes such that several particle diameters fit into the channel height, the interaction signal, seen in Figs. 5 and 6, forms one of four different types. The first, null type, is where no signal is recorded at all. We disregard this type here. This leaves 3 types of signal, which can be demonstrated using a simple simulation and are shown in Fig. 9, which were calculated for the positions in the flow indicated in Fig. 8. Due to the narrow size of the detector in the vertical dimension (~500 nm), at height (z) values greater than one bead radius, light from rays falling directly onto the detectors are no longer interrupted by the beads. Consequently, interactions at these z values tend to result in only a very small positive going signal as the beads redirect otherwise divergent rays back within the acceptance angle of the detector as shown by the lower signal in Fig. 9. These events are rare and extracting an accurate bead size from them is not trivial. They have therefore been omitted from the following analysis. The other two data types where a particle simply blocks light falling onto the detector (upper trace of Fig. 9) or where at the central position the particle enhances the light falling on the detector through focussing the laser light (middle trace) can both be used to determine particle diameter.

Figure 10 is a histogram of bead size for the mixed sample calculated by applying equation [1] to the 101 transit events recorded between t = 5 s and t = 35 s in Fig. 5 assuming the width is simply the width of the laser, 10um.

As expected the measured size distribution of the beads is bimodal with peaks centred on 10 and 15 microns. The distribution of size values around each of the peaks however is

Optics EXPRESS

asymmetrically spread towards smaller sizes. This is a result of using a fixed beam width in Eq. (1).

To correct for the bead width measurement error that results from differences in vertical bead position, we define a system response function, Eq. (2), that narrows linearly from its widest point on the central optical axis, at z = 0, to zero a vertical distance Δz from this point, as indicated in Fig. 8:

$$R(z) = \begin{cases} \frac{1}{n \times \Delta z}(z - z_0) & if \quad z_0 < z < (z_0 + \Delta z) \\ 0 & otherwise \end{cases} \qquad (2)$$

where n is a normalisation constant and z is vertical position from the central optical axis.

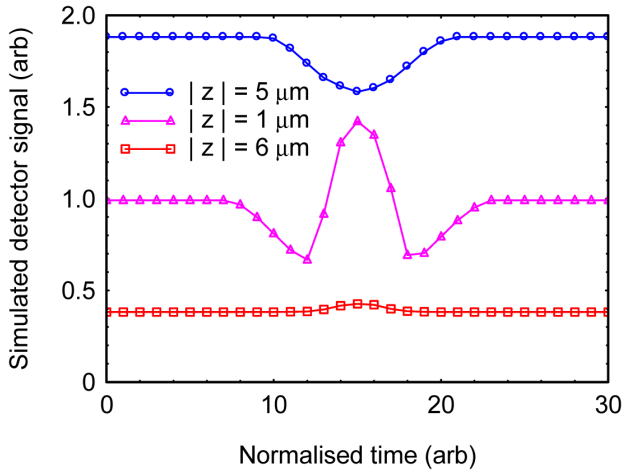

Fig. 9. Three different event durations generated by simulating 10 μm beads passing through the beam at the three different vertical heights (indicated by the three blue spheres with coloured arrows in Fig. 8).

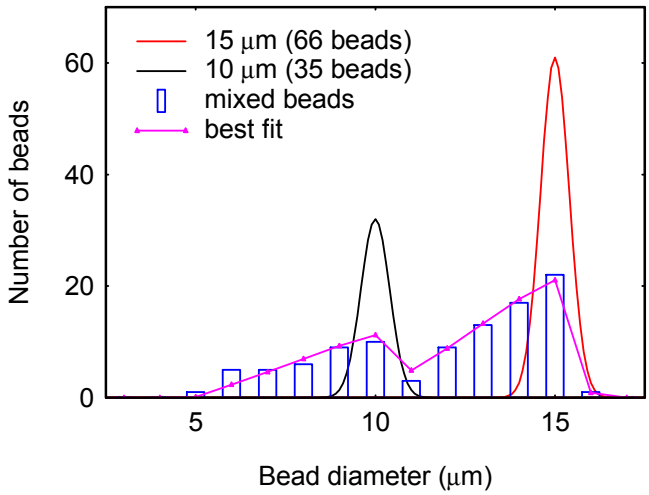

Fig. 10. Histogram of bead diameter measured for the mixed bead sample (blue bars) assuming w is equal to the laser/detector ridge width, 10 μm and a best fit line (purple triangles) to this data obtained by convolution of a beam width function and two separate Gaussian distributions for the 10 μm and 15 μm beads (red and black lines respectively.)

Optics EXPRESS

By performing a convolution of the system response function with Gaussian distributions for each of the bead sizes, a best fit for the mixed bead size histogram data in Fig. 10 can be found. From the resulting fitting parameters, the two size distributions can clearly be resolved allowing the number of beads in each distribution to be estimated as sixty six 15 μm beads and thirty five 10 μm beads. The sensitivity of the on-chip measurement to positional variations is corrected here using the system response function. Alternatively, the channel depth could be better matched to particle size or an active method of position control such as dielectrophoresis [26] could be implemented to minimise the effect. The sensitivity to position could also be used to advantage. With further analysis it could provide valuable information about the position of particles in the fluid flow and, combined with the local velocity measurement, useful information about the fluid itself. Furthermore, individual particles can be tracked as they pass through the detector array. Comparison of correlated transit events could potentially provide information about a particle's orientation and/or sphericity.

We do not show data here but have observed signal for microbeads as small as 0.5 μm. However, with the current layout it is difficult to unambiguously detect whether an event is caused by a single 10 μm object or a cluster of smaller objects. By using lasers of smaller width we expect to be able to improve the resolution to small particles down to a width of 1-2um where diffraction becomes significant. The upper limit on the size of particle that can be detected is ultimately set by the dimensions of the micro-channel. The largest channels that we have produced to date are 40 μm deep by 50 μm wide.

The data supporting the results in this paper can be found at http://doi.org/10.17035/d.2017.0033945197.

5. Conclusions

Chip based particle sensing using 3D capillary fill microfluidics integrated with monolithically integrated lasers and photodetectors has been used to demonstrate the feasibility of true chip scale photonic measurements of fluids. The approach is scalable and manufactured using industry standard compound semiconductor fabrication tools. 3D micro-channels on deep etched photonic integrated substrates were formed in SU-8 photoepoxy using wavelength selective UV lithography. SU-8 was treated with O2 plasma and ethanolamine to facilitate capillary action for water based fluids. The need for fluid speed regulation via external pumps was removed by measuring local particle velocity at the point of interrogation and particle position within the fluid flow was derived from multiple time resolved forward scattered light signals. Particle size discrimination of 10 and 15 μm polystyrene microbeads was demonstrated as an example of the potential of this truly small scale and manufacturable integrated platform for optical measurements of fluids and the particles they contain.

Funding

This work was supported by EPSRC grant EP/L005409/1.